PCCP

Accepted Manuscript

ROYAL SOCIETY OF CHEMISTRY

www.rsc.org/pccp

Phys. Chem. Chem. Phys.

COMMUNICATION

Preparation and Lithium Storage Performance of Yolk-Shell Si@Void@C Nanocomposites

Received 00th January 20xx,
Accepted 00th January 20xx

DOI: 10.1039/x0xx00000x

www.rsc.org/

Liwei Su,[a†] Jian Xie,[a†] Yawei Xu,[a] Lianbang Wang,[a*] Yuanhao Wang,[b*] and Manman Ren[c]

Yolk-shell Si@void@C nanocomposites are prepared via a facile method of resorcinol-formaldehyde coating and LiOH etching, without SiO_2 pre-modification on Si particles, expensive carbon sources, or environmentally-unfriendly HF solutions. Profiting from the favorable features, Si@void@C nanocomposites exhibit considerable reversible capacities (628 mAh g^{-1} after 100 cycles) and good rate performances.

Tesla Motors' plans, building its own lithium-ion battery (LIB) factory for electric vehicles (EVs), have caused a stir in the battery industry since 2014.[1] To meet the dramatically increasing demands of the high-energy-density LIBs for EVs, it is an effective strategy to develop advanced anode materials with ultrahigh reversible capacities to substitute for the commercial graphite.[2, 3] Among dozens of substitutions, silicon is an extremely competitive candidate owing to various advantages such as the abundance, safety, environmental friendliness, low operation potential (<0.5 V vs. Li/Li^+) and in particular, the ever-known highest theoretical capacity (~4200 mAh g^{-1}, for $Li_{22}Si_5$ alloys).[4-6] On the other hand, it simultaneously suffers from troublesome shortcomings, including the sluggish diffusivity for Li^+ ions (1.9×10^{-14} cm^2 s^{-1}),[7] intrinsically low electric conductivity (1.6×10^{-3} S m^{-1})[8] and in particular, huge volume variations (>400%) leading to the gradual cracking, pulverization, electrical disconnection, unstable solid electrolyte interphase (SEI) films, and resultantly a rapid capacity fading.

To approach these issues mentioned above, great efforts have been made in both the external and internal aspects. For the external ones, developing novel binders instead of the conventional polyvinylidene difluoride (PVDF) can effectively sustain the electrode integrity and electric connection during large volume swings between Si and Li_xSi alloys. Besides, introducing suitable electrolyte additives including vinylene carbonate (VC) and fluoroethylene carbonate (FEC) can stabilize the solid-electrolyte interface (SEI) films in the battery system.[9, 10] For the internal factors, preparing Si with favorable architectures (such as nanosized,[11, 12] porous,[13-15] and/or hollow structures[16-18]) can greatly shorten the diffusion path of electron/Li^+ ions, promote the Li-Si reactions, and reduce the absolute volume swings. Furthermore, combining Si with stable and high-conductivity materials and especially preparing Si@C core-shell nanostructures, can effectively improve the electron transport, accommodate the volume expansion, and attenuate the direct contact between Si and the electrolyte at the same time.[19-24]

However, traditional core-shell Si@C composites cannot provide enough space to accommodate the unavoidable volume expansion for Li-Si alloying. In the last few years, yolk-shell structured Si@void@C composites were proposed as a preferable strategy. The voids can offer passivation space for the volume swelling, while the carbon shells can enhance the electric conductivity and minimize the loss of Si particles. For instance, Cui *et al.* prepared ultra-high-performance Si@void@C nanocomposites by etching the SiO_2 intermediate layers of the core double-shelled $Si@SiO_2@C$ precursors with HF solutions.[25-28] As a substitute route, Cho's group fabricated Si@void@C composites by directly etching core-shell Si@C precursors with Fe^{3+} assisted HF solutions.[29] More recently, Si@void@C composites were also synthesized by directly etching the Si cores in Si@C precursors with NaOH[30, 31] or HF[32] aqueous solutions. In these methods, however, it is inevitable to involve the SiO_2 layers, expensive carbon sources (e.g., dopamine), and/or HF solutions, making the synthesis complicated, high-cost, and environmentally unfriendly. Note that, Zhang's group developed a facile method to prepare Si@void@C nancomposites via citric acid

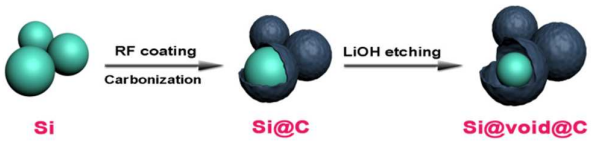

Scheme 1. Schematic diagram for the preparation process of yolk-shell Si@void@C nanocomposites.

[a] State Key Laboratory Breeding Base of Green Chemistry-Synthesis Technology, College of Chemical Engineering, Zhejiang University of Technology, Hangzhou 310014, China E-mail: wanglb99@zjut.edu.cn
[b] Renewable Energy Research Group (RERG), Department of Building Services Engineering, the Hong Kong Polytechnic University, Room: FJ715, Kowloon, Hong Kong E-mail: bewang@polyu.edu.hk
[c] Institute of Materials Science and Engineering, Qilu University of Technology, Jinan 250353, China
† Both authors contributed equally to this work.

Electronic Supplementary Information (ESI) available: Experimental details, TGA curves for the Si@C and Si@void@C nanocomposites, TEM images of Si@void@C electrodes after 30 cycles, TEM images and electrochemical performances of Si@C nanocomposites with different LiOH etching times. See DOI: 10.1039/x0xx00000x

coating on the mesoporous Si from the magnesiothermic reduction of SiO_2. Based on the "balloon" mechanism, voids can be formed through the expansion of air in the mesopourous Si and the inflations of citric acid layers during the carbonization.[33]

In this work, to obtain yolk-shell Si@void@C nanocomposites, Si nanoparticles were directly and uniformly encapsulated with cheap resorcinol-formaldehyde (RF) resin and further etched with eco-friendly LiOH solutions (as illustrated in **Scheme 1**). Besides the merits inheriting from core-shell Si@C nanostructures, yolk-shell Si@void@C nanocomposites possessed an essential space to accommodate the huge expansion of Si-Li alloying. As a result, Si@void@C nanocomposites exhibited much higher reversible capacities (628 mAh g^{-1} after 100 cycles) and rate performances than pure Si and Si@C composites. This work can help us develop advanced synthesis methods for yolk-shell structured materials and enlighten us on understanding their structure merits for energy storage and other promising applications.

X-ray diffraction (XRD) analysis was carried out to identify the crystallinity nature of the samples (**Figure 1**). Taking together, all the samples demonstrated similar diffraction patterns except the peak intensity. The strong peaks at 28°, 47°, 56°, 69°, and 76° can be well assigned to the (1 1 1), (2 2 0), (3 1 1), (4 0 0), and (3 3 1) planes of the standard card of cubic Si (JCPDS 27-1402), respectively. The weakened peak intensity of Si@C and Si@void@C nanocomposites came from the reduced Si contents of 71 wt.% and 67 wt.%, respectively, which can be confirmed by thermogravimetric analysis (TGA) in air (**Figure S1**). The additional broad peak at 20-25° in the Si@C and Si@void@C nanocomposites corresponded to the amorphous carbon shells. No other characteristic peaks can be observed for any impurities.

Figure 2 showed the morphology and structure of raw Si, Si@C, and Si@void@C nanocomposites. SEM images displayed that Si particles in each sample had the similar spherical shapes and particle size distributions (generally 50-100 nm) (**Figures 2A-C**). After RF coating and carbonization, all the Si nanoparticles were completely encapsulated by well-proportioned carbon shells (~10 nm in thickness) (**Figure 2D**). These core-shell Si@C nanoparticles tightly connected with each other to form an excellent network for electron transport. **Figures 2E**, **F** further confirmed that, with the help of LiOH etching, the Si nanocores were uniformly downsized with ~4 wt.% loss of Si confirmed by TGA, and resulted in ~10-nm-thick voids between the Si cores and carbon shells. It is clear that all the Si

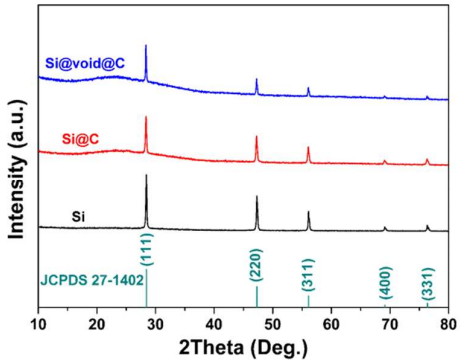

Figure 1. XRD patterns of the samples: raw Si nanoparticles, core-shell Si@C and yolk-shell Si@void@C nanocomposites.

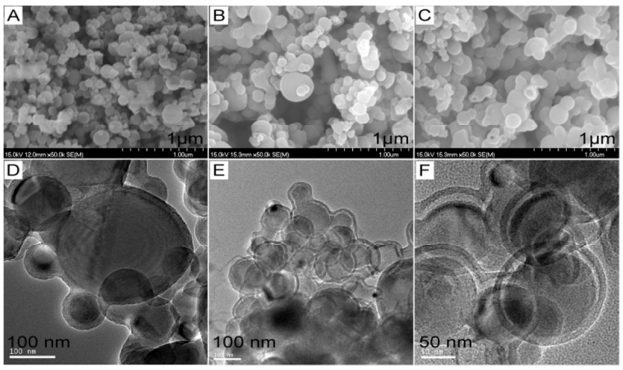

Figure 2. SEM images of (A) raw Si nanoparticles, (B) Si@C, and (C) Si@void@C; TEM images of (D) Si@C and (E, F) Si@void@C.

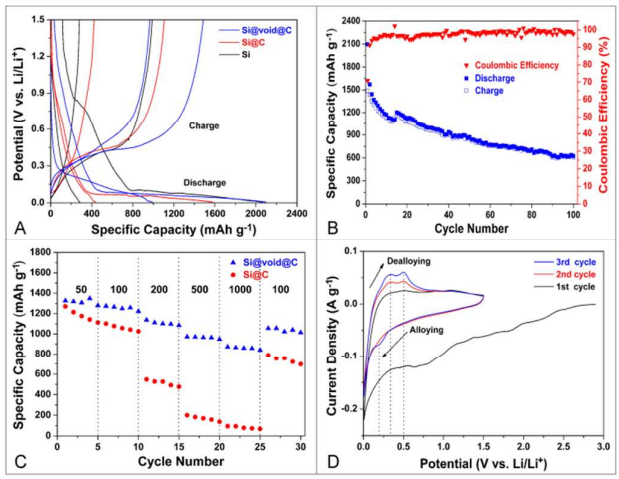

Figure 3. (A) Discharge-charge profiles of raw Si, Si@C, and Si@void@C electrodes for the 1st and 30th cycles and (B) long-term cycling performances of Si@void@C electrodes at 50 mA g^{-1}. (C) Rate performances of Si@C and Si@void@C electrodes. (D) Cyclic voltammetry (CV) curves for Si@void@C electrodes.

nanoparticles were well pent up in the reinforced-concrete and high-conductivity carbon frameworks, which can not only promote the electron transfer but also attenuate the direct contact between Si and the electrolyte. The voids can effectively buffer the unavoidable volume expansions of the Si-Li alloying and maintain the support integrity of composites. Furthermore, the Si cores and the voids can be controlled by optimizing the etching times (**Figure S2**).

Profiting from the favorable yolk-shell structures, Si@void@C nanocomposites demonstrated promising reversible capacities and rate performances (**Figure 3**). Note that all the presented capacities were based on the entire weight of samples. **Figure 3A** showed galvanostatic discharge–charge curves of pure Si, core-shell Si@C, and yolk-shell Si@void@C electrodes for the 1st and 30th cycles. Obviously, Si@void@C displayed a much better characteristic potential plateau of Si-Li redox reactions. The voltage slope at 1.5-0.15 V can be ascribed to the formation of SEI films, which mainly occurred in the first discharge process and resulted in large capacities. The long plateau below 0.15 V mainly belonged to the lithiation of Si and C, whereas the platform at ~0.4 V corresponded to the delithiation process. The initial charge capacity (ICC) of the raw Si was 987 mAh g^{-1} and rapidly decreased to 278 mAh g^{-1} after

Table 1. Comparison on the preparation methods and performances of yolk-shell Si@void@C composites between previous reports and this work.

Refs	Si size (nm)	Carbon source	Methods	Si[a] (%)	VC[b] or FEC[c] involved	Binders	Current (mA g^{-1})	RC[d] (mAh g^{-1})
28	100	Polystyrene	HF-SiO_2	47	No	None	1000	872 (x=200)
27	50	Acetylene	HF-SiO_2	30	Yes	CMC[e]	1000	654 (x=100)
25	100	Dopamine	HF-SiO_2	71	Yes	SA[f]	4000	1500(x=1000)
34	50	Dopamine	HF-SiO_2	48	Yes	CMC	2000	528 (x=300)
29	100	Fe-phthalocyanine	HF-Si	63	Yes	CMC-PAA[g]	200	1500 (x=50)
31	100	Dopamine	NaOH-Si	75	Yes	CMC	1000	804 (x=50)
32	100	Polyacrylonitrile	HF-Si	65	No	SA	250	700 (x=100)
35	2-5	Sucrose	HF-SiO_2	38	Yes	CMC-SBR[h]	2500	720 (x=1000)
36	100	Polyvinylchloride	HF-SiO_2	21	No	PVDF[i]	200	350 (x=20)
30	500	Dopamine	NaOH-SiO_2	44	No	PVDF	200	530 (x=100)
33	150	Citric acid (CA)	Inflations of CA	64	No	PVDF	100	1265 (x=150)
37	100	Toluene	HF-SiO_2	37	No	PVDF	100	767 (x=100)
26	100	Sucrose	HF-SiO_2	28	No	PVDF	50	618 (x=20)
This work	50-100	RF	LiOH-Si	67	No	PVDF	50	628 (x=100)

[a] The Si content in the composites; [b] VC: vinylene carbonate; [c] FEC: fluoroethylene carbonate; [d] RC: reversible capacity after x cycles; [e] CMC: sodium carboxymethyl cellulose; [f] SA: sodium alginate; [g] PAA: poly(acrylic acid); [h] SBR: styrene-butadiene rubber; [i] PVDF: polyvinylidene difluoride.

30 cycles due to lacking of ideal conductivity and structure stability. Benefiting from the carbon shells, Si@C electrodes presented an increased ICC of 1106 mAh g^{-1} and a reversible capacity of 422 mAh g^{-1} after 30 cycles. By sharp contrast, the ICC of Si@void@C electrodes was 1487 mAh g^{-1} and still maintained 967 mAh g^{-1} after 30 cycles and 628 mAh g^{-1} after 100 cycles (**Figure 3B**). The initial Coulombic efficiency of Si@viod@C was ~71%, much higher than that of raw Si and Si@C, grew up to ~91% for the second cycle and held at ~98% hereafter. When the current densities increased stepwise from 50 to 100, 200, 500, and 1000 mA g^{-1}, the average reversible capacities were approximately 1320, 1230, 1100, 965, and 860 mAh g^{-1}, respectively (**Figure 3C**). As the rate returned to 100 mA g^{-1}, an average capacity of 1056 mAh g^{-1} could be recovered. Cyclic voltammetry (CV) measurements were carried out to further illustrate the electrochemical behaviors of Si@void@C electrodes (**Figure 3D**). The broad cathodic peak at ~0.7 V in the first cycle was assigned to the SEI formation, while the peak at ~0.15 V corresponded to the Si-Li alloying, consistent with the discharge-charge profiles. The peak at ~0.38 V in the first anodic curve, belonging to the de-alloying of Li_xSi, became stronger and separated into two peaks at ~0.34 and 0.50 V in following cycles, indicating that the alloying/de-alloying of Si-Li proceeded via a solid-solution mechanism and gradually transformed to a two-phase reaction.[38] Note that, the yolk–shell structure still maintained even after 30 cycles at 500 mA g^{-1} (**Figure S3**).

Table 1 summarized the preparation methods and electrochemical performances of yolk-shell Si@void@C composites. Up to now, the synthesis of Si@void@C can be mainly classified into 3 strategies: (i) removing the intermediate SiO_2 layers of the core double-shelled Si@SiO_2@C precursors[25-28, 34-37]; (ii) directly etching Si cores in core-shell Si@C composites by HF[29, 32] or NaOH[31] solutions; and (iii) coating and carbonization of citric acid layers on mesoporous Si according to the "balloon" mechanism.[33] In these methods except the third, however, it is inevitable to introduce the SiO_2 intermediate layers, expensive carbon sources (such as dopamine), and/or environmentally-unfriendly HF solutions. Differently in this work, uniform Si@C nanocomposites were successfully synthesized in the RF solutions without any pre-modification of Si surface. In addition, LiOH aqueous solution was adopted as a preferable choice to substitute for HF. Note that, the binders and the additives in the electrolytes played an important role in improving the lithium storage capability.[25, 27, 29, 31, 34, 35] Otherwise, the performances of Si-based anodes were greatly limited.[26, 36, 37] By contrast, even in the traditional test system, yolk-shell Si@void@C nanocomposites herein still demonstrated promising reversible capacities (628 mAh g^{-1} after 100 cycles) and considerable rate performances. Besides, we also investigated the effect of etching times on the structure and electrochemical performances of samples (**Figure S4**).

In summary, yolk-shell Si@void@C nanocomposites were prepared via a facile RF coating and subsequent LiOH etching. Different with previous methods, the route in this work avoided the introduction of SiO_2 intermediate layers, expensive carbon sources, and environmentally unfriendly HF solutions. The obtained Si@void@C nanocomposites possessed uniform space between Si nanocores (generally 50-100 nm) and carbon nanoshells (~10 nm thick). The size of the Si cores and the voids can be controlled by optimizing the etching times. Profiting from the yolk-shell features, Si@void@C exhibited much better reversible capacities (628 mAh g^{-1} after 100 cycles) and rate performances than that of pure Si and traditional core-shell Si@C nanocomposites. This work can enlighten us on exploiting advanced preparation methods for yolk-shell structured materials and understanding their structure merits for energy storage and other promising applications.

Notes and references

This work was supported by the International Science and Technology Cooperation Program of Zhejiang Province (2012C14027), the Promotive Research Fund for Excellent Young Scientists of Shandong Province (BS2013NJ006), and the National Natural Science Foundation of China (21403195).

1. C. Martin, *Nat. Nanotechnol.*, 2014, **9**, 327-328.
2. H. Bai, C. Li and G. Shi, *Adv. Mater.*, 2011, **23**, 1089-1115.
3. H.-H. Li, X.-L. Wu, H.-Z. Sun, K. Wang, C.-Y. Fan, L.-L. Zhang, F.-M. Yang and J.-P. Zhang, *J. Phys. Chem. C*, 2015, **119**, 3495-3501.
4. K. Li, H. Xie, J. Liu, Z. Ma, Y. Zhou and D. Xue, *Phys. Chem. Chem. Phys.*, 2013, **15**, 17658-17663.
5. J. E. Cloud, Y. Wang, T. S. Yoder, L. W. Taylor and Y. Yang, *Angew. Chem. Int. Ed.*, 2014, **53**, 14527-14532.
6. B. A. Boukamp, G. C. Lesh and R. A. Huggins, *J. Electrochem. Soc.*, 1981, **128**, 725-729.
7. C. S. Fuller and J. C. Severiens, *Phys. Rev.*, 1954, **96**, 21-24.
8. E. M. Conwell, *Proceedings of the IRE*, 1952, **40**, 1327-1337.
9. S. Uchida, M. Yamagata and M. Ishikawa, *J. Electrochem. Soc.*, 2015, **162**, A406-A412.
10. V. Etacheri, O. Haik, Y. Goffer, G. A. Roberts, I. C. Stefan, R. Fasching and D. Aurbach, *Langmuir*, 2012, **28**, 965-976.
11. H. Ma, F. Cheng, J. Y. Chen, J. Z. Zhao, C. S. Li, Z. L. Tao and J. Liang, *Adv. Mater.*, 2007, **19**, 4067-4070.
12. X. Li, C. Yan, J. Wang, A. Graff, S. L. Schweizer, A. Sprafke, O. G. Schmidt and R. B. Wehrspohn, *Adv. Energy Mater.*, 2015, DOI: 10.1002/aenm.201401556.
13. H. Kim, B. Han, J. Choo and J. Cho, *Angew. Chem. Int. Ed.*, 2008, **47**, 10151-10154.
14. P. Zhang, L. Wang, J. Xie, L. Su and C.-a. Ma, *J. Mater. Chem. A*, 2014, **2**, 3776-3782.
15. P. Gao, H. Jia, J. Yang, Y. Nuli, J. Wang and J. Chen, *Phys. Chem. Chem. Phys.*, 2011, **13**, 20108-20111.
16. X. Huang, J. Yang, S. Mao, J. Chang, P. B. Hallac, C. R. Fell, B. Metz, J. Jiang, P. T. Hurley and J. Chen, *Adv. Mater.*, 2014, **26**, 4326-4332.
17. J. Deng, H. Ji, C. Yan, J. Zhang, W. Si, S. Baunack, S. Oswald, Y. Mei and O. G. Schmidt, *Angew. Chem. Int. Ed.*, 2013, **52**, 2326-2330.
18. L. Zhang, J. Deng, L. Liu, W. Si, S. Oswald, L. Xi, M. Kundu, G. Ma, T. Gemming, S. Baunack, F. Ding, C. Yan and O. G. Schmidt, *Adv. Mater.*, 2014, **26**, 4527-4532.
19. L. Su, Z. Zhou and M. Ren, *Chem. Commun.*, 2010, **46**, 2590-2592.
20. S. Sim, P. Oh, S. Park and J. Cho, *Adv. Mater.*, 2013, **25**, 4498-4503.
21. L. Su, Y. Jing and Z. Zhou, *Nanoscale*, 2011, **3**, 3967-3983.
22. M. Zhou, F. Pu, Z. Wang, T. Cai, H. Chen, H. Zhang and S. Guan, *Phys. Chem. Chem. Phys.*, 2013, **15**, 11394-11401.
23. P. Gao, J. Fu, J. Yang, R. Lv, J. Wang, Y. Nuli and X. Tang, *Phys. Chem. Chem. Phys.*, 2009, **11**, 11101-11105.
24. Y. Q. Sun, Q. O. Wu and G. Q. Shi, *Energy Environ. Sci.*, 2011, **4**, 1113-1132.
25. N. Liu, H. Wu, M. T. McDowell, Y. Yao, C. Wang and Y. Cui, *Nano Lett.*, 2012, **12**, 3315-3321.
26. X.-y. Zhou, J.-j. Tang, J. Yang, J. Xie and L.-l. Ma, *Electrochim. Acta*, 2013, **87**, 663-668.
27. X. Li, P. Meduri, X. Chen, W. Qi, M. H. Engelhard, W. Xu, F. Ding, J. Xiao, W. Wang, C. Wang, J.-G. Zhang and J. Liu, *J. Mater. Chem.*, 2012, **22**, 11014-11017.
28. H. Wu, G. Zheng, N. Liu, T. J. Carney, Y. Yang and Y. Cui, *Nano Lett.*, 2012, **12**, 904-909.
29. Y. Park, N.-S. Choi, S. Park, S. H. Woo, S. Sim, B. Y. Jang, S. M. Oh, S. Park, J. Cho and K. T. Lee, *Adv. Energy Mater.*, 2013, **3**, 206-212.
30. Y. Ru, D. G. Evans, H. Zhu and W. Yang, *RSC Adv.*, 2014, **4**, 71-75.
31. L. Pan, H. Wang, D. Gao, S. Chen, L. Tan and L. Li, *Chem. Commun.*, 2014, **50**, 5878-5880.
32. C. Pang, H. Song, N. Li and C. Wang, *RSC Adv.*, 2015, **5**, 6782-6789.
33. H.-H. Li, J.-W. Wang, X.-L. Wu, H.-Z. Sun, F.-M. Yang, K. Wang, L.-L. Zhang, C.-Y. Fan and J.-P. Zhang, *RSC Adv.*, 2014, **4**, 36218–36225.
34. S. Chen, M. L. Gordin, R. Yi, G. Howlett, H. Sohn and D. Wang, *Phys. Chem. Chem. Phys.*, 2012, **14**, 12741-12745.
35. T. Jaumann, M. Herklotz, M. Klose, K. Pinkert, S. Oswald, J. Eckert and L. Giebeler, *Chem. Mater.*, 2015, **27**, 37-43.
36. S. Iwamura, H. Nishihara and T. Kyotani, *J. Phys. Chem. C*, 2012, **116**, 6004-6011.
37. H. Tao, L. Z. Fan, W. L. Song, M. Wu, X. He and X. Qu, *Nanoscale*, 2014, **6**, 3138-3142.
38. C. Gao, H. Zhao, P. Lv, C. Wang, J. Wang, T. Zhang and Q. Xia, *J. Electrochem. Soc.*, 2014, **161**, A2216-A2221.